Final Project Report

Tanzina Taher Ifty (G01569073) & Chetan Vallabhaneni (G01588972)

Fall 2025 Linear Systems and Control (ECE-521-001, ECE-521-P01)
George Mason University

Date: December 08, 2025

Project Topic

Comparative Controller Design for Inverted Pendulum Stabilization

Paper Reference

Paper 1: Kumar, P., O. N. Mehrotra, and J. Mahto. "Controller design of inverted pendulum using pole placement and LQR." International Journal of Research in Engineering and Technology (2012): 532-538.

Paper 2: Lim, Yon Yaw, Choon Lih Hoo, and Yen Myan Felicia Wong. "Stabilising an inverted pendulum with PID controller." MATEC web of conferences. Vol. 152. EDP Sciences, 2018.

Objective

The main objectives of this project are outlined as follows:

- Derive the nonlinear equations of motion for the Quanser IP02 inverted pendulum using the Euler–Lagrange formulation.
- Linearize the dynamics about the upright equilibrium to obtain a four-state state-space model suitable for controller design.
- Analyze key system properties of the linearized model, including stability, controllability, and observability.
- Implement and tune a PID controller on the reduced 2×2 pendulum-only model to illustrate fundamental control concepts.

- Design a full-state Pole Placement controller for the 4×4 linearized model.
- Design an LQR controller for the same state-space representation, optimizing both state deviation and control effort.
- Repeat the controller synthesis and simulation using two distinct sets of hardware parameters (long pendulum and short pendulum) to assess robustness and parameter sensitivity.
- Simulate all controllers in MATLAB/Simulink under identical initial conditions and compare their performance.
- Evaluate controller behavior using quantitative metrics including settling time, overshoot, steady-state error, and control effort.

System Description

The inverted pendulum system studied in this project is based on the Quanser IP02 linear cart platform equipped with two possible pendulum configurations: a long 24-inch pendulum and a shorter half-length pendulum. The cart is actuated by a DC motor through a gearbox and pinion–rack mechanism, enabling horizontal translation along a linear track. A rigid pendulum is mounted to the cart through a low-friction rotary pivot, allowing rotational motion in the vertical plane.

- **Actuation:** The system is actuated by a single control input—the motor voltage—which generates a horizontal force on the cart. This force indirectly influences the pendulum angle through dynamic coupling.
- **Pendulum Modeling:** The pendulum is modeled as a rigid rod characterized by its mass, center of mass location, moment of inertia, full length, and rotational damping. Two parameter sets corresponding to the long and short pendulum assemblies are used in this project to evaluate controller robustness.
- **Underactuated Dynamics:** The system is underactuated because control is applied only to the cart position while the pendulum angle evolves through nonlinear coupling. As a result, stabilizing the pendulum in the upright position requires coordinated motion of the cart.
- **Sensing and State Feedback:** The onboard sensors measure cart position and pendulum angle. These measurements, along with their derivatives, form the four-state representation used for full-state control design (Pole Placement and LQR).
- **Instability of Upright Equilibrium:** The pendulum's upright configuration is an unstable equilibrium. Without closed-loop control, even small perturbations grow over time, causing the pendulum to fall.

- **Complex Nonlinear Behavior:** The coupled translational–rotational motion introduces nonlinear and highly sensitive dynamics, making the inverted pendulum a standard benchmark for evaluating modern control strategies, particularly those requiring fast, precise, and robust stabilization.

Figure 1: Quanser IP02 cart with long inverted pendulum setup.

Hardware Parameters

The physical parameters of the Quanser IP02 cart and both inverted pendulum configurations (long and short pendulum modules) used in this project are listed below in Table **??**. These two datasets represent official Quanser hardware specifications and are used for comparative controller design and analysis.

Table 1: Hardware parameters for the two Quanser IP02 configurations.

Parameter	**Set 1: Long Pendulum**	**Set 2: Short Pendulum**
Cart mass M [kg]	0.94	0.57
Cart friction b [N·s/m]	0.050	0.050
Pendulum mass m [kg]	0.230	0.127
Pendulum length L_p [m]	0.6413	0.324
COM distance l [m]	0.3302	0.170
Inertia (COM) $J_{p,cm}$ [kg·m^2]	7.8838×10^{-3}	1.66×10^{-3}
Inertia (pivot) I [kg·m^2]	0.03294	0.00533
Pendulum damping B_p	0.0024	0.0024
Gravity g [m/s^2]	9.81	9.81

Nonlinear Modeling Using Euler–Lagrange Equations

The inverted pendulum system is modeled using the Euler–Lagrange formulation, which is well suited for deriving the equations of motion of mechanical systems with coupled translational and rotational dynamics. The independent generalized coordinates chosen for this system are:

$$x(t) \quad \text{(cart position)}, \qquad \theta(t) \quad \text{(pendulum angle, clockwise positive)}.$$

Kinetic and Potential Energy

The kinetic energy consists of the translational motion of the cart, and the combined translational and rotational motion of the pendulum:

$$T = \frac{1}{2}M\dot{x}^2 + \frac{1}{2}m\left(\dot{x} + l\dot{\theta}\cos\theta\right)^2 + \frac{1}{2}I\dot{\theta}^2.$$

The potential energy of the pendulum, referenced with the upright position at $\theta = 0$, is:

$$V = -mgl\cos\theta.$$

The Lagrangian is then defined as:

$$L = T - V.$$

Euler–Lagrange Equations

The dynamics are obtained using the Euler–Lagrange equation for each coordinate $q_i \in \{x, \theta\}$:

$$\frac{d}{dt}\left(\frac{\partial L}{\partial \dot{q}_i}\right) - \frac{\partial L}{\partial q_i} = Q_i,$$

where Q_i represents non-conservative generalized forces. In this system,

$$Q_x = F - b\dot{x}, \qquad Q_\theta = -B_p\dot{\theta}.$$

Applying the Euler–Lagrange formulation yields the nonlinear coupled equations of motion:

$$(M+m)\ddot{x} + ml\ddot{\theta}\cos\theta - ml\dot{\theta}^2\sin\theta + b\dot{x} = F,$$
$$(I+ml^2)\ddot{\theta} + ml\ddot{x}\cos\theta + mgl\sin\theta + B_p\dot{\theta} = 0.$$

These equations describe the full nonlinear dynamics of the inverted pendulum system. They will be linearized about the upright equilibrium in the next section to obtain a state-space model suitable for controller design.

Present the derivation of the nonlinear equations of motion.

Linearization About Upright Equilibrium

To design linear controllers, the nonlinear equations of motion must be linearized about the upright equilibrium position. The equilibrium occurs at:

$$\theta = 0, \qquad \dot{\theta} = 0, \qquad \dot{x} = 0, \qquad F = 0.$$

Small-Angle Approximations

For small deviations around the upright position, the following approximations are used:

$$\sin\theta \approx \theta, \qquad \cos\theta \approx 1, \qquad \dot{\theta}^2 \approx 0.$$

Applying these approximations to the nonlinear equations of motion results in the linearized coupled equations:

$$(M+m)\ddot{x} + ml\ddot{\theta} + b\dot{x} = F,$$
$$(I+ml^2)\ddot{\theta} + ml\ddot{x} + mgl\,\theta + B_p\dot{\theta} = 0.$$

Solving for $\ddot{x}$ and $\ddot{\theta}$

The linearized equations can be written in matrix form:

$$\begin{bmatrix} M+m & ml \\ ml & I+ml^2 \end{bmatrix} \begin{bmatrix} \ddot{x} \\ \ddot{\theta} \end{bmatrix} = \begin{bmatrix} F - b\dot{x} \\ -mgl\,\theta - B_p\dot{\theta} \end{bmatrix}.$$

The determinant of the mass matrix is:

$$p = (M+m)(I+ml^2) - (ml)^2.$$

Solving for the accelerations:

$$\ddot{x} = \frac{(I+ml^2)(F-b\dot{x}) + m^2gl^2\theta + mlB_p\dot{\theta}}{p},$$

$$\ddot{\theta} = \frac{-ml(F-b\dot{x}) - mgl(M+m)\theta - B_p(M+m)\dot{\theta}}{p}.$$

These linearized equations form the basis for constructing the state-space model in the next section.

State-Space Model

Using the derived linearized equations and the final hardware parameters, the system is written in the state-space form

$$\dot{x} = Ax + Bu, \qquad y = Cx + Du,$$

with the state vector and input defined as:

$$x = \begin{bmatrix} x \\ \dot{x} \\ \theta \\ \dot{\theta} \end{bmatrix}, \qquad u = F.$$

The coefficients of the state-space matrices were computed using:

$$p = (M+m)(I+ml^2) - (ml)^2,$$

$$a_{22} = -\frac{b(I+ml^2)}{p}, \qquad a_{23} = \frac{m^2 g l^2}{p},$$

$$a_{42} = \frac{ml\,b}{p}, \qquad a_{43} = -\frac{mgl(M+m)}{p},$$

$$b_2 = \frac{I+ml^2}{p}, \qquad b_4 = -\frac{ml}{p}.$$

Numerical State-Space Matrices (24-inch Long Pendulum)

Substituting all physical parameters into the formulas above yields the following matrices:

$$A = \begin{bmatrix} 0 & 1 & 0 & 0 \\ 0 & -0.0467 & 0.9106 & 0 \\ 0 & 0 & 0 & 1 \\ 0 & 0.0611 & -14.0284 & 0 \end{bmatrix}, \qquad B = \begin{bmatrix} 0 \\ 0.9340 \\ 0 \\ -1.2222 \end{bmatrix},$$

$$C = \begin{bmatrix} 1 & 0 & 0 & 0 \\ 0 & 0 & 1 & 0 \end{bmatrix}, \qquad D = \begin{bmatrix} 0 \\ 0 \end{bmatrix}.$$

These matrices represent the complete linearized model of the inverted pendulum system and are used for the design of the PID, Pole Placement, and LQR controllers.

Numerical State-Space Matrices (Short Pendulum Configuration)

Using the short-pendulum parameter set, the resulting linearized state-space model is:

$$A_{\text{short}} = \begin{bmatrix} 0 & 1 & 0 & 0 \\ 0 & -0.0775 & 0.7874 & 0 \\ 0 & 0 & 0 & 1 \\ 0 & 0.1859 & -25.4203 & 0 \end{bmatrix}, \qquad B_{\text{short}} = \begin{bmatrix} 0 \\ 1.5499 \\ 0 \\ -3.7177 \end{bmatrix}.$$

$$C = \begin{bmatrix} 1 & 0 & 0 & 0 \\ 0 & 0 & 1 & 0 \end{bmatrix}, \qquad D = \begin{bmatrix} 0 \\ 0 \end{bmatrix}.$$

These matrices describe the complete linearized dynamics of the short pendulum configuration and are used for full controller redesign and comparison against the long pendulum system.

System Properties

The stability, controllability, and observability of the inverted pendulum system were evaluated using the eigenvalues and matrix ranks of the linearized state-space models for both hardware configurations (24-inch long pendulum and short pendulum).

Stability

For the **24-inch long pendulum** (Set 1), the eigenvalues of A_1 are:

$$\lambda(A_1) = \{\, 0,\ -0.0427,\ -0.0020 \pm 3.7454i \,\}.$$

The zero eigenvalue corresponds to the freely moving cart, while the complex conjugate pair with small negative real parts indicates an oscillatory and **open-loop unstable** mode, characteristic of upright pendulum dynamics.

For the **short pendulum** (Set 2), the eigenvalues of A_2 are:

$$\lambda(A_2) = \{0,\ -0.0717,\ -0.0029 \pm 5.0418i\}.$$

The larger imaginary part reflects a **higher natural frequency**, meaning the short pendulum oscillates faster and is even more unstable. As expected, the upright equilibrium remains **open-loop unstable** for both parameter sets.

Controllability

The controllability matrices for both systems,

$$\mathcal{C}_i = [\, B_i \ A_i B_i \ A_i^2 B_i \ A_i^3 B_i \,], \quad i = 1, 2,$$

satisfy:

$$\operatorname{rank}(\mathcal{C}_1) = 4, \qquad \operatorname{rank}(\mathcal{C}_2) = 4.$$

Thus, both configurations are **fully controllable**, meaning the applied cart force can influence all four states.

Observability

The observability matrices,

$$\mathcal{O}_i = \begin{bmatrix} C \\ CA_i \\ CA_i^2 \\ CA_i^3 \end{bmatrix}, \quad i = 1, 2,$$

yield:

$$\text{rank}(\mathcal{O}_1) = 4, \qquad \text{rank}(\mathcal{O}_2) = 4.$$

Therefore, the outputs (cart position and pendulum angle) are sufficient to reconstruct the entire system state, and both configurations are **fully observable**.

Controller Design

PID Controller

Motivation for Using a Simplified Model

Classical PID control operates using a single error signal, typically the pendulum angle θ, and therefore cannot access or regulate the full state $(x, \dot{x}, \theta, \dot{\theta})$ of the cart–pendulum system. Since the Quanser IP02 is a fourth-order, underactuated, and open-loop unstable system, a single-loop PID controller is fundamentally incapable of stabilizing the full dynamics. To apply PID meaningfully and consistently with prior literature, we follow the reference paper and work with a reduced model in which the cart dynamics are removed, yielding a single-degree-of-freedom rotational pendulum.

Simplified Pendulum Model

Neglecting cart motion, the nonlinear dynamics simplify to

$$J\ddot{\theta} = m_p g l\, \theta + u,$$

where u is a generalized control torque. Linearizing about the upright equilibrium gives

$$\ddot{\theta} = a\,\theta + b\,u, \qquad a = \frac{m_p g l}{J}, \qquad b = \frac{1}{J}.$$

With the parameters of the Quanser pendulums,

$$\text{Set 1 (Long): } m_p = 0.23 \text{ kg},\ l = 0.3302 \text{ m},\ J = 7.8838\times10^{-3} \text{ kg}\cdot\text{m}^2,$$

$$\text{Set 2 (Short): } m_p = 0.127 \text{ kg},\ l = 0.170 \text{ m},\ J = 4.254\times10^{-3} \text{ kg}\cdot\text{m}^2,$$

the state-space representation for each pendulum is

$$\dot{x} = \begin{bmatrix} 0 & 1 \\ a & 0 \end{bmatrix} x + \begin{bmatrix} 0 \\ b \end{bmatrix} u, \qquad x = \begin{bmatrix} \theta \\ \dot{\theta} \end{bmatrix}.$$

PID Tuning Methodology

We employ the same iterative PID tuning procedure as the reference paper, evaluating three progressively richer controllers:

- **Iteration 1 (P Control):** $u(t) = K_p e(t)$.
- **Iteration 2 (PD Control):** $u(t) = K_p e(t) + K_d \dot{e}(t)$.
- **Iteration 3 (Full PID):** $u(t) = K_p e(t) + K_d \dot{e}(t) + K_i \int e(t)\, dt$.

The initial condition for both pendulum configurations was set to

$$\theta(0) = 0.15 \text{ rad} \approx 8.6^\circ,$$

matching the disturbance used in the reference study.

Because the long and short pendulums exhibit different dynamic behavior, the PID controller was tuned separately for each case. The final gains that produced stable and well-damped responses were:

$$\text{Set 1 (Long Pendulum):} \qquad K_p = 1.20,\ K_d = 0.09,\ K_i = 0.30,$$

$$\text{Set 2 (Short Pendulum):} \qquad K_p = 1.10,\ K_d = 0.06,\ K_i = 0.25.$$

Simulation Results

Iteration 1: P Control Figure 2 shows that proportional control alone cannot stabilize either pendulum. The long pendulum (Set 1) diverges rapidly, while the shorter pendulum (Set 2) oscillates but remains bounded due to lower inertia and gravitational torque.

Iteration 2: PD Control Adding derivative action significantly increases damping (Fig. 3). Both pendulums stabilize, but Set 1 exhibits a slower and more oscillatory decay, consistent with its larger length and inertia. Set 2 converges rapidly with small overshoot.

Iteration 3: Full PID Control With the addition of integral action (Fig. 4), both systems converge smoothly to zero steady-state error. Set 2 again settles more quickly, while Set 1 shows a longer transient response.

PID Comparison Across Pendulum Sets Figure 5 directly compares the PID-controlled angle trajectories. As expected, the long pendulum exhibits larger overshoot and slower damping due to higher inertia and gravitational torque. Figure 6 shows that the control effort for the two pendulums is nearly identical, with only minor differences in the early transient.

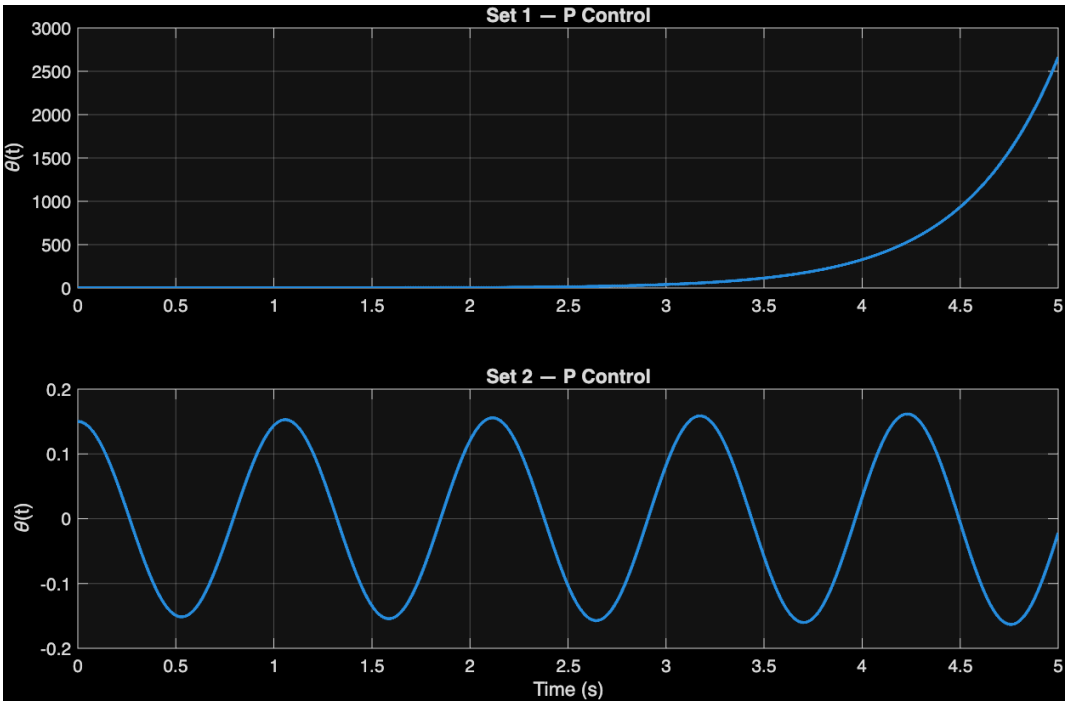

Figure 2: P-only control for Set 1 and Set 2. Set 1 diverges rapidly while Set 2 shows bounded oscillatory behavior.

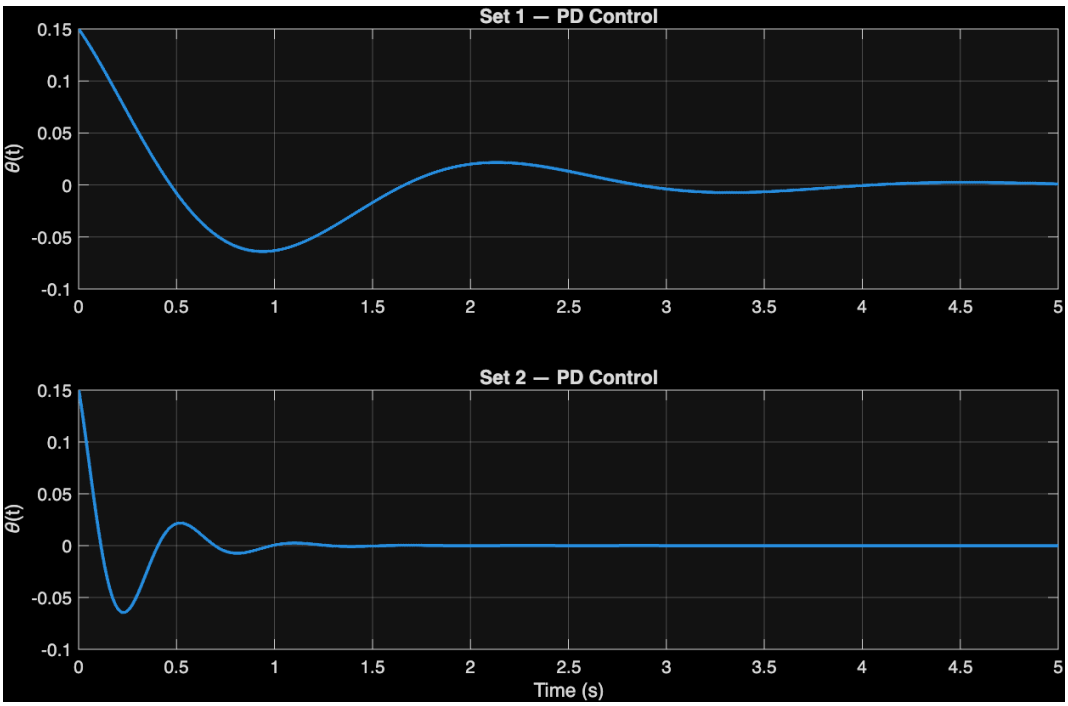

Figure 3: PD control greatly increases damping. Both pendulums stabilize, with Set 2 settling more quickly.

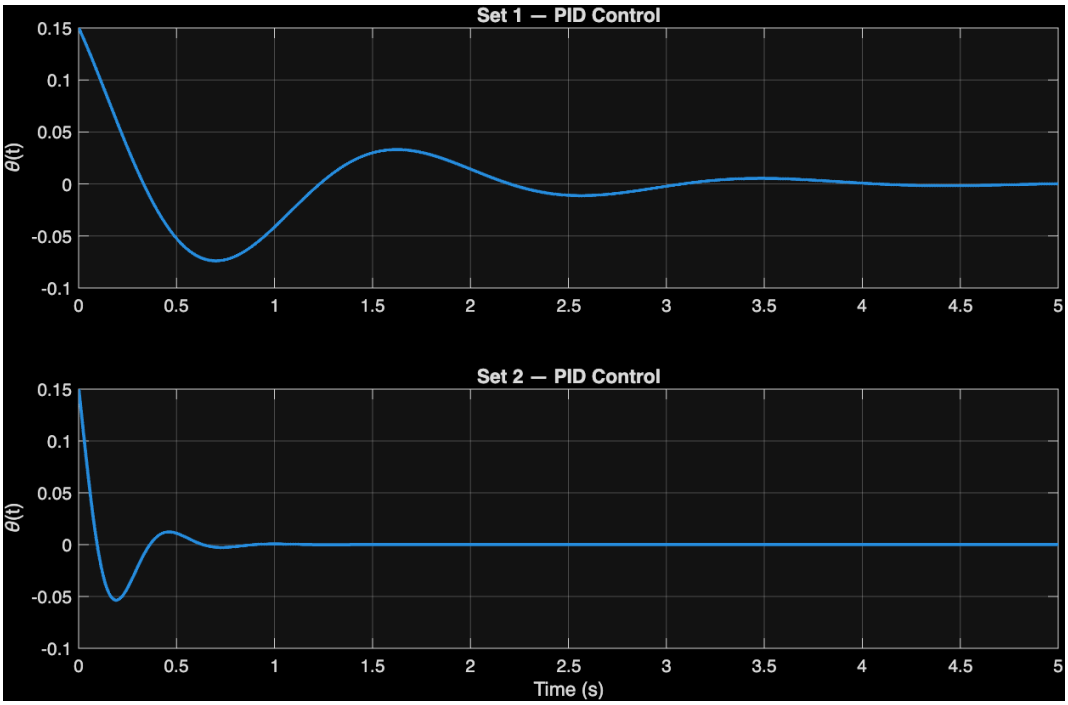

Figure 4: PID control results for Set 1 and Set 2. Integral action eliminates steady-state error for both models.

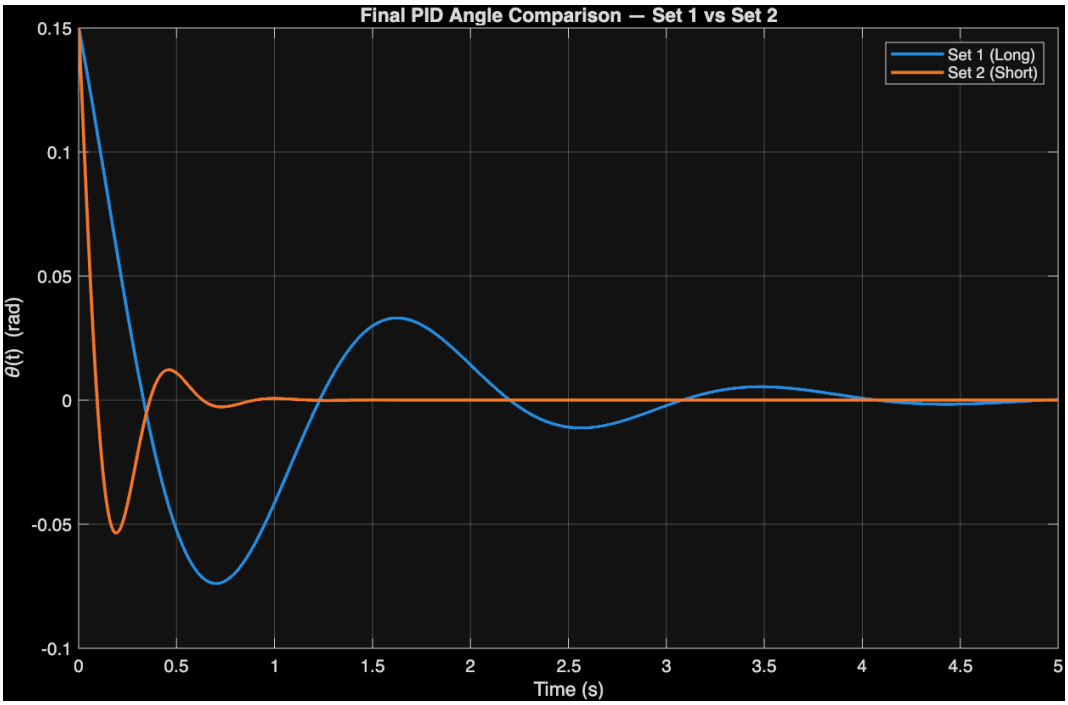

Figure 5: Final PID angle trajectory comparison. The long pendulum shows larger overshoot and slower damping.

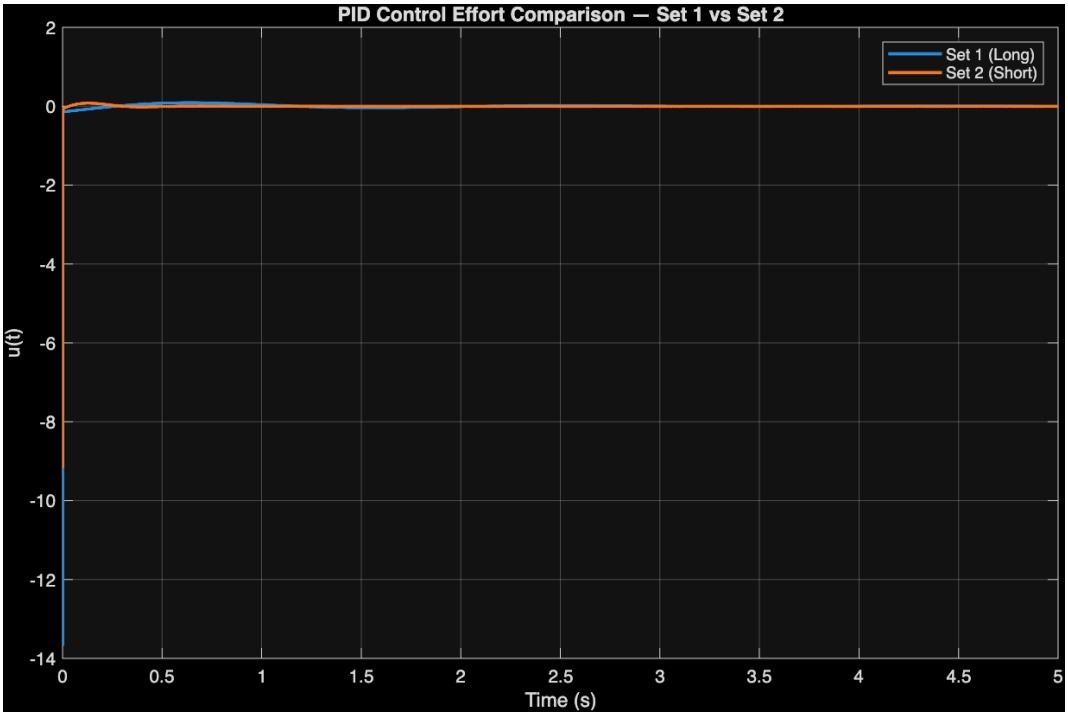

Figure 6: Control effort comparison under the tuned PID controller. Both pendulums receive nearly identical initial control inputs.

Pole Placement Controller

Pole placement provides a direct method for shaping the closed-loop dynamics of the inverted pendulum by selecting desired pole locations and computing a state-feedback gain K such that the eigenvalues of $(A - BK)$ match the specified values. Since both state-space models (Set 1: long pendulum, Set 2: short pendulum) were shown to be fully controllable in the System Properties section, pole placement is feasible for both configurations.

Selection of Desired Closed-Loop Poles

The design specifications follow the same criteria used in the reference paper: a desired settling time of approximately $T_s \approx 1\,\text{s}$ with about 10% overshoot. These performance targets correspond to a second-order system with damping ratio ζ and natural frequency ω_n satisfying

$$M_p = e^{-\frac{\zeta\pi}{\sqrt{1-\zeta^2}}} = 0.10,$$

which yields

$$\zeta \approx 0.591.$$

Using the 2% settling-time formula,

$$T_s = \frac{4}{\zeta\omega_n},$$

and substituting $T_s = 1$ gives

$$\omega_n = \frac{4}{0.591} \approx 6.76 \text{ rad/s}.$$

The dominant poles are then computed as

$$s_{1,2} = -\zeta\omega_n \pm j\,\omega_n\sqrt{1-\zeta^2} = -4 \pm j\,5.4553.$$

To ensure rapid decay of the remaining modes in the fourth-order system, two additional real poles were placed deeper in the left-half plane following the common "5× and 10×" guideline:

$$s_3 = -20, \qquad s_4 = -40.$$

The complete desired pole set is therefore

$$p_{\text{des}} = \{-4 \pm j\,5.4553,\ -20,\ -40\}.$$

State-Feedback Gains for Each Parameter Set

Using MATLAB's `place` function with the respective linearized matrices for Set 1 (long pendulum) and Set 2 (short pendulum), the pole-placement gains were obtained as follows:

$$K_1 = [\,3053.34 \;\; 762.75 \;\; 1260.09 \;\; 527.29\,],$$

$$K_2 = [\,1003.75 \;\; 250.71 \;\; 68.69 \;\; 86.25\,].$$

In both cases, the eigenvalues of the closed-loop matrices $(A_i - B_i K_i)$ exactly matched the desired pole locations, confirming successful pole placement for each configuration.

Simulation Results

Both controllers were evaluated from the same initial condition,

$$x(0) = [\,0,\ 0,\ 0.15,\ 0\,]^T,$$

representing a 0.15 rad initial pendulum deflection.

Pendulum Angle Response. Figure 7 shows the pendulum angle trajectories for both parameter sets. Both controllers stabilize the pendulum rapidly with small overshoot, consistent with the designed pole locations. The short pendulum (Set 2), being lighter and lower inertia, settles slightly faster and with reduced oscillatory motion.

Cart Position Response. Figure 8 compares the cart motion for both parameter sets. The long pendulum requires larger cart excursions (up to about 0.12 m) to counteract its higher inertia, while the short pendulum requires significantly smaller motion (less than 0.04 m). Both trajectories converge smoothly back toward the origin.

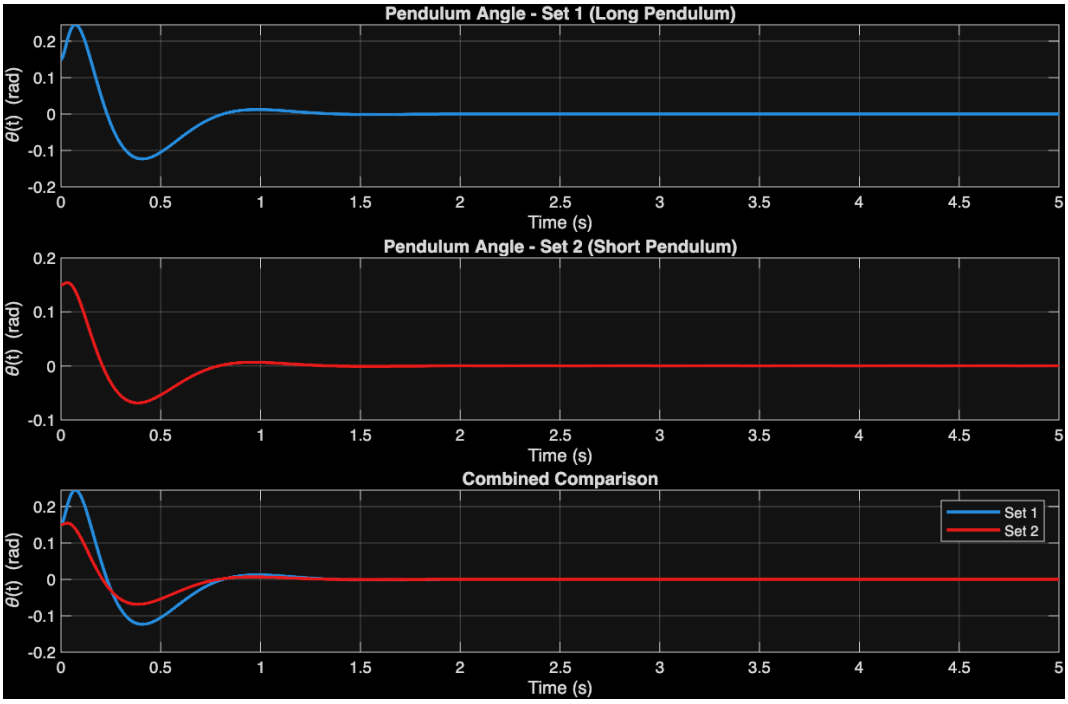

Figure 7: Pendulum angle response under pole placement for Set 1 (long pendulum) and Set 2 (short pendulum). Both systems stabilize quickly with small overshoot, with Set 2 settling slightly faster.

Control Effort. Figure 9 shows the control inputs $u(t) = -Kx(t)$ for both sets. The long pendulum requires significantly higher initial force (nearly -200 N) due to its larger inertia and longer moment arm, whereas the short pendulum requires much less (approximately ± 10 N). In both cases, the force quickly decays to near zero as the system stabilizes.

Overall, pole placement stabilizes both pendulum configurations quickly and reliably. The primary observed differences arise from physical parameter variations: the short pendulum settles faster, moves the cart less, and requires smaller control effort.

LQR Controller

The Linear Quadratic Regulator (LQR) provides an optimal state–feedback controller for stabilizing the cart–pendulum system by minimizing a quadratic cost on the state deviation and control effort. Unlike PID control, which uses only the pendulum angle error, the LQR controller utilizes the full state vector

$$x = [\, x,\ \dot{x},\ \theta,\ \dot{\theta}\,]^T,$$

making it well suited for regulating the inherently unstable and coupled cart–pendulum dynamics.

The control input is computed as

$$u(t) = -Kx(t),$$

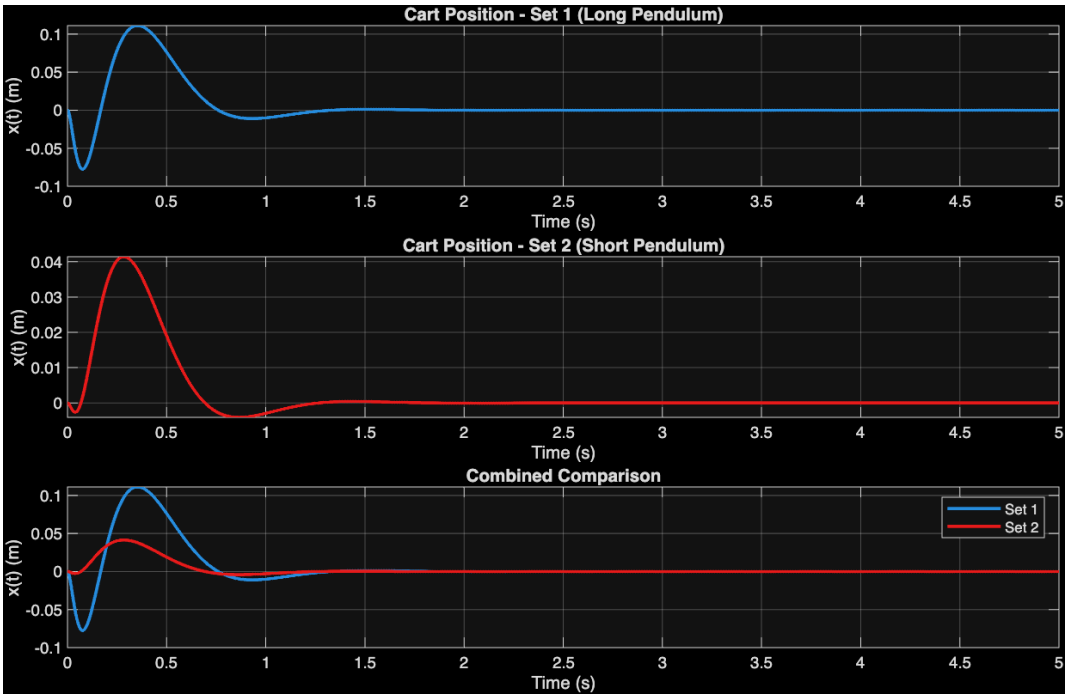

Figure 8: Cart position response (Pole Placement) for Set 1 and Set 2. The long pendulum requires greater corrective motion, while the short pendulum stabilizes with smaller displacement.

where the gain matrix K minimizes the infinite–horizon cost function

$$J = \int_0^\infty \left(x^T Q x + R u^2\right)\, dt,$$

with $Q \succeq 0$ penalizing deviations in the states and $R > 0$ penalizing excessive control effort.

Selection of Q and R

A three–step iterative tuning procedure was used to progressively improve stability, damping, and control smoothness. The same weighting matrices were applied to both pendulum configurations (Set 1 and Set 2) so that their relative behaviours could be compared under identical design conditions.

$$\begin{aligned} Q_1 &= \mathrm{diag}(35,\ 150,\ 0.1,\ 1), \quad R_1 = 2, \\ Q_2 &= \mathrm{diag}(30,\ 2,\ 50,\ 250), \quad R_2 = 10, \\ Q_3 &= \mathrm{diag}(40,\ 20,\ 300,\ 40), \quad R_3 = 12. \end{aligned}$$

The final weighting matrices (Q_3, R_3) provided the best balance between pendulum stability, cart motion, and control effort. These same matrices were then applied to both system models.

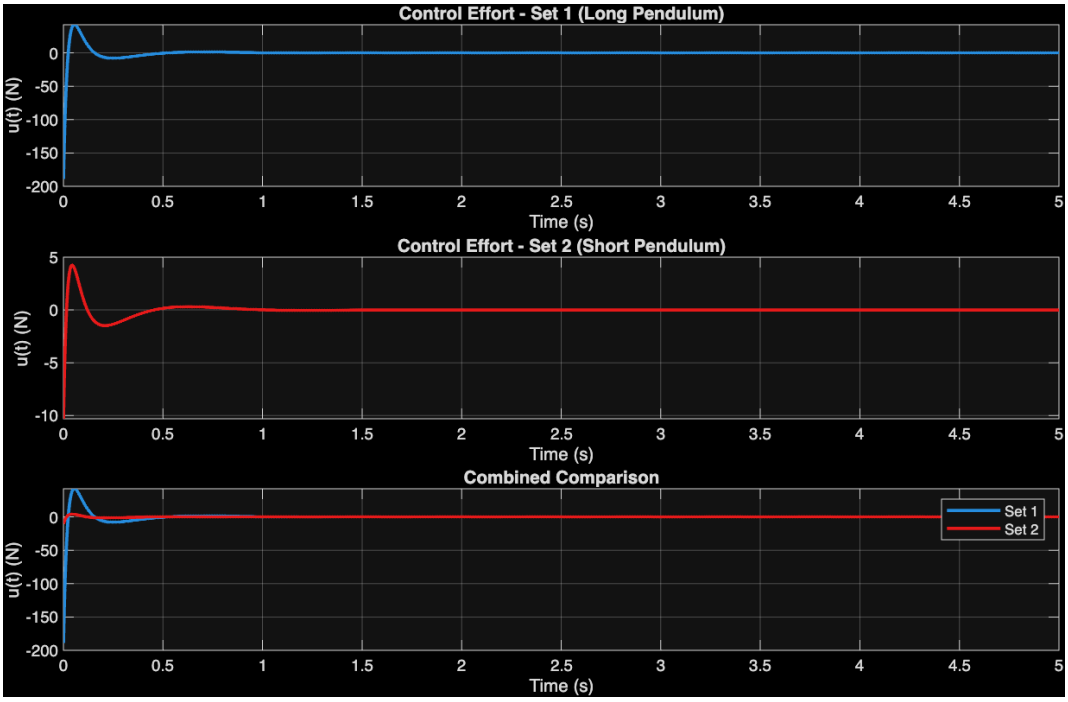

Figure 9: Control effort (Pole Placement) for Set 1 and Set 2. The long pendulum demands a much larger initial force, while the short pendulum stabilizes the system using comparatively small actuator effort.

Final LQR Gains

Using the Set 1 and Set 2 linearized models, the final LQR gains were:

$$K_1 = \begin{bmatrix} 1.826 & 2.728 & -4.763 & -1.670 \end{bmatrix}, \qquad \text{(Set 1: Long Pendulum)}$$

$$K_2 = \begin{bmatrix} 1.826 & 2.483 & -5.910 & -1.630 \end{bmatrix}, \qquad \text{(Set 2: Short Pendulum)}$$

The first gain element is the same for both systems due to identical cart dynamics, while the remaining terms differ because the short pendulum (Set 2) has higher natural frequency and requires stronger stabilization of the angular states.

The closed–loop eigenvalues for both systems lie strictly in the left-half plane, confirming that the LQR controllers successfully stabilize both pendulum configurations.

Simulation Results

The controllers were tested from an initial condition

$$x(0) = [\,0,\ 0,\ 0.15,\ 0\,]^T,$$

representing an initial 0.15 rad pendulum deviation.

Figures 10–12 show the resulting angle response, cart motion, and control effort for both systems.

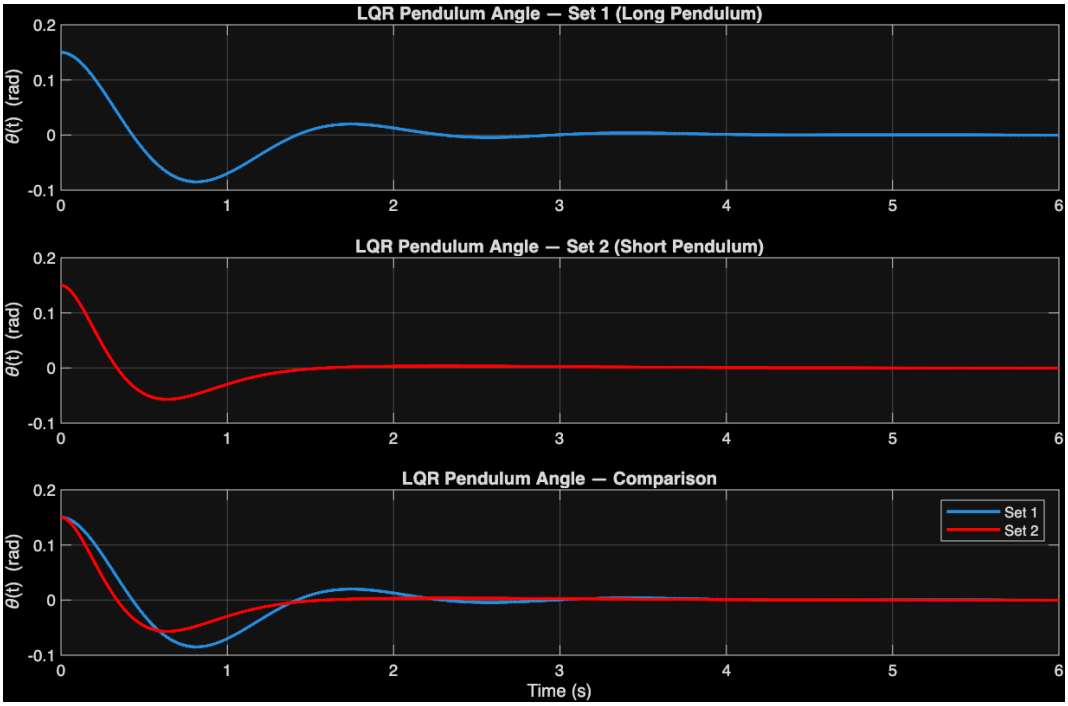

Figure 10: LQR pendulum angle response for Set 1 (top), Set 2 (middle), and combined comparison (bottom). Both controllers stabilize the pendulum smoothly with similar settling times.

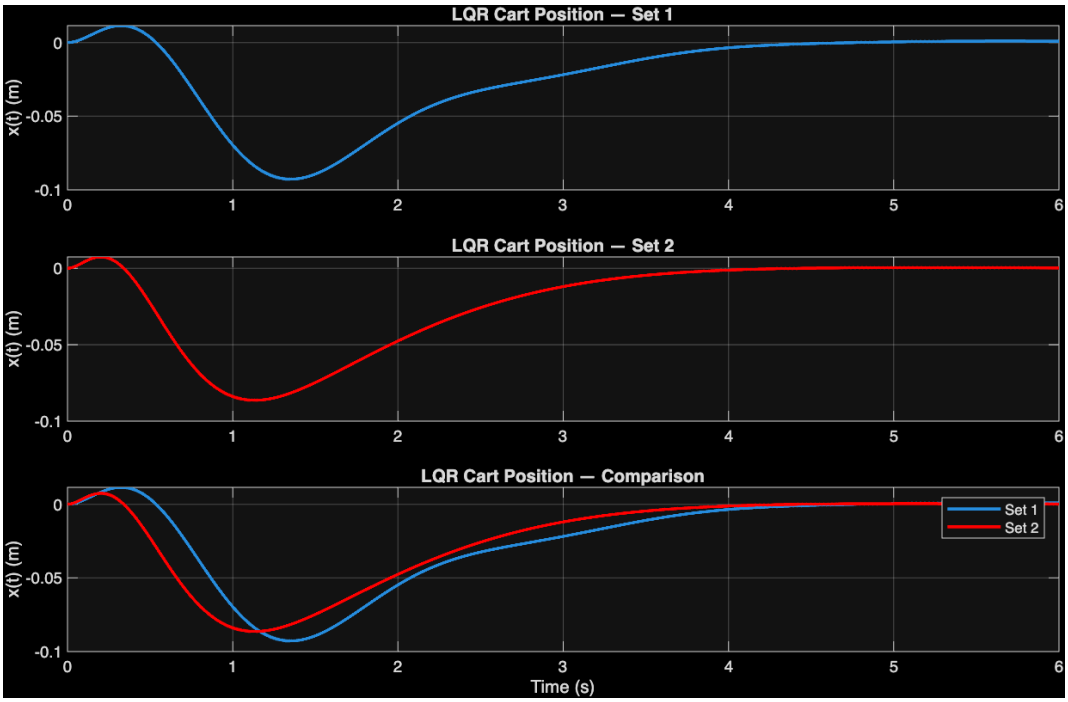

Figure 11: Cart position response under LQR control. Both pendulum configurations produce similar cart excursions of approximately 10 cm during stabilization.

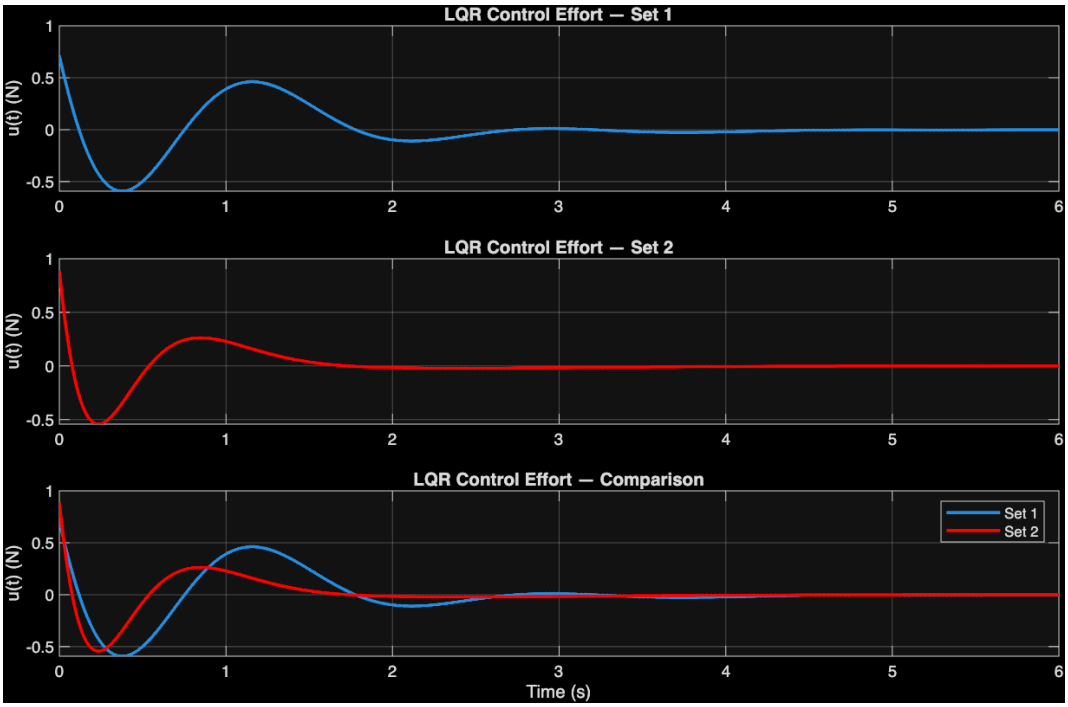

Figure 12: Control effort (LQR) comparison for both pendulum configurations. The short pendulum (Set 2) requires slightly less input due to its lower inertia.

Overall, both LQR controllers achieve smooth, stable regulation of the inverted pendulum. The short pendulum stabilizes slightly faster due to its higher natural frequency, while the long pendulum exhibits slower but equally stable convergence.

Comparison of Full-State Controllers

This section compares the performance of the Pole Placement and LQR controllers on both parameter sets of the Quanser IP02 inverted pendulum system:

$$\text{Set 1: Long pendulum,} \qquad \text{Set 2: Short pendulum.}$$

All simulations use the same nonzero initial angle $\theta(0) = 0.15$ rad, with the full-state initial condition

$$x(0) = [0 \;\; 0 \;\; 0.15 \;\; 0]^T.$$

The PID controller is intentionally excluded from this comparison because it is applied to a reduced two-state pendulum model and cannot act on the cart dynamics required for true stabilization of the full inverted-pendulum system.

0.1 Pendulum Angle Response

Figures 13 and 14 show the pendulum angle response for both controller designs and both parameter sets.

For both long- and short-pendulum configurations, the Pole Placement controller yields the fastest initial correction. The steep transient response reflects the aggressively selected poles, which emphasize rapid stabilization at the expense of control effort. In Set 1 (long pendulum), this results in a pronounced impulse-like action immediately after startup, which quickly moves the pendulum toward the equilibrium orientation. In Set 2 (short pendulum), the faster natural dynamics further amplify this behavior, producing an even quicker trajectory back toward the upright position.

The LQR controller exhibits a smoother and more gradually decaying angular response. The overshoot is significantly smaller, the oscillations damp out more gently, and the response exhibits strong robustness against parameter differences between Set 1 and Set 2. Both controllers achieve zero steady-state error, but LQR accomplishes this with a far less aggressive transient, yielding a cleaner and more hardware-friendly angle trajectory overall.

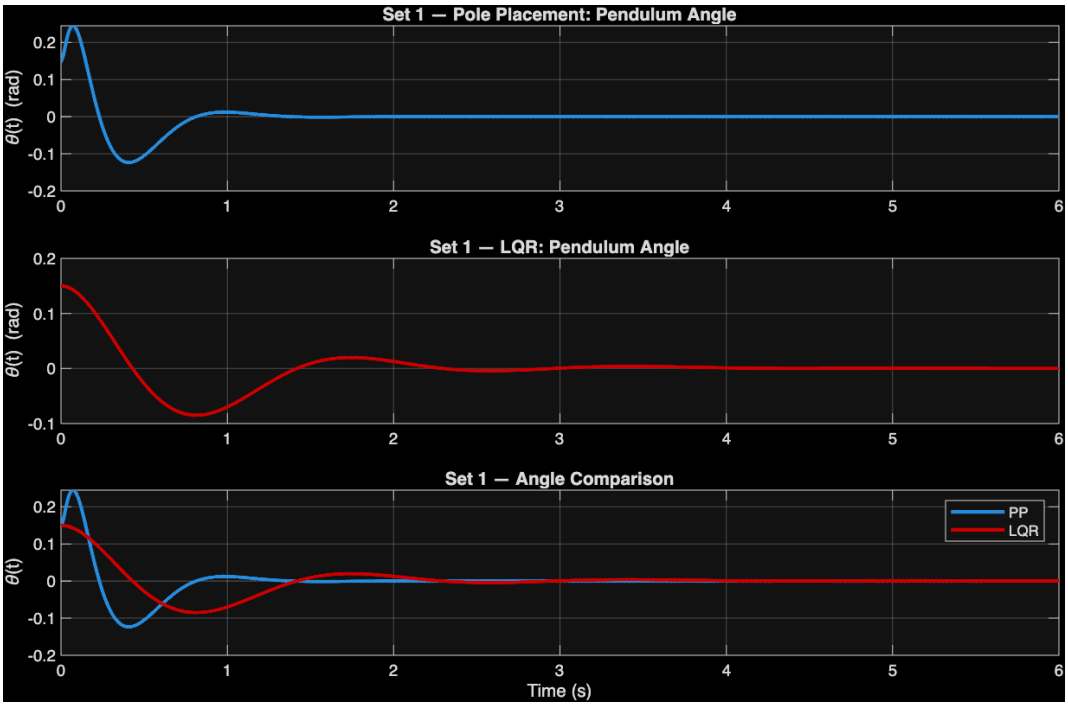

Figure 13: Set 1 (Long Pendulum): Pendulum angle comparison between Pole Placement and LQR.

0.2 Cart Position Response

Cart displacement for both controller designs is shown in Figures 15 and 16. Because cart movement is the actuator's only means of influencing the pendulum angle, this metric directly reflects how each controller regulates the coupled dynamics.

In Set 1 (long pendulum), the Pole Placement controller forces the cart to move rapidly in the initial phase, producing large and abrupt displacements. The system settles quickly but exhibits significant impulsive motion. This can be unacceptable in hardware because the cart is constrained by rail length, friction, and motor limits.

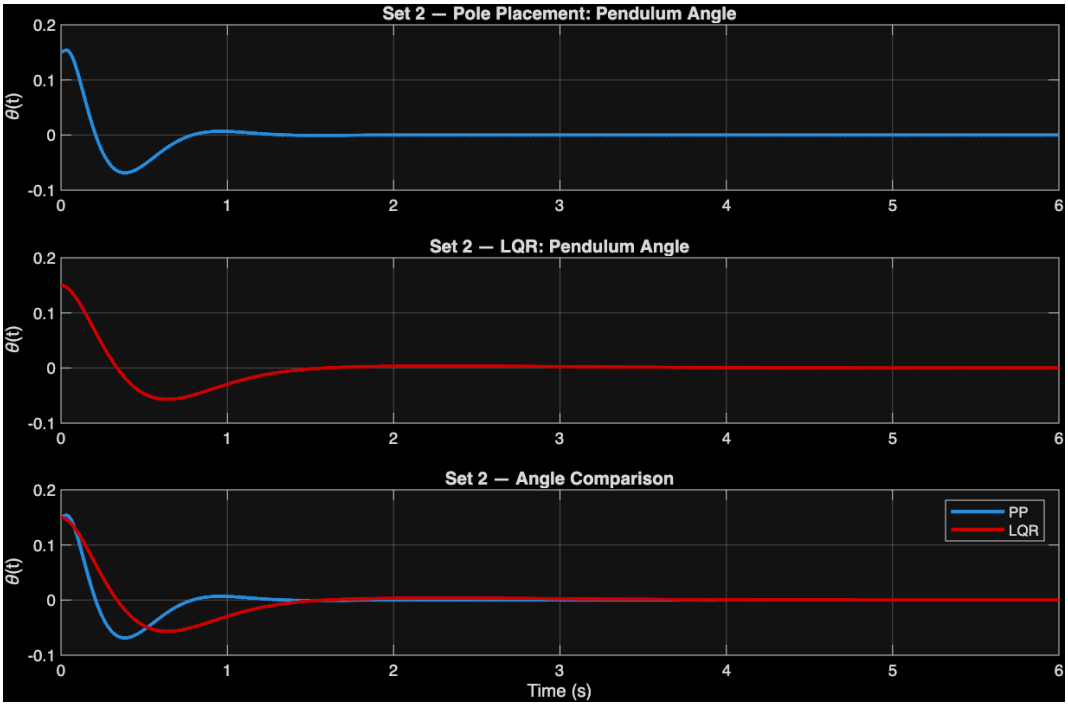

Figure 14: Set 2 (Short Pendulum): Pendulum angle comparison between Pole Placement and LQR.

The LQR controller yields a slower yet markedly smoother trajectory. Although the cart moves farther than in the Pole Placement design during the first two seconds, the motion is continuous and well damped, without the sharp velocity reversals seen in the Pole Placement implementation. This results in safer and more predictable behavior.

In Set 2 (short pendulum), the required cart motion is generally smaller because the shorter pendulum has a stronger natural restoring torque. Both controllers reflect this, but the structural difference remains: Pole Placement is sharp and aggressive, while LQR is smooth and gradual.

0.3 Control Effort Comparison

Control effort $u(t)$ is shown in Figures 17 and 18. This metric directly exposes feasibility in real hardware, where actuator saturation and current limits are critical.

Pole Placement consistently demands extremely large peak inputs. In Set 1 (long pendulum), the initial force reaches nearly -200 N, and in Set 2 (short pendulum) about -10 N. Although these forces drive very fast regulation, they exceed the capabilities of IP02 actuators and would immediately saturate the motor. Such impulsive behavior also risks mechanical stress, rail collisions, and unstable closed-loop motion on the physical system.

By contrast, the LQR controller requires less than 1 N in both parameter sets. This dramatic difference highlights the effect of the input-weighting term in the LQR cost function, which discourages unnecessarily large actuator efforts. The resulting input trajectory is continuous, smooth, low-energy, and ideally suited for systems with tight physical constraints.

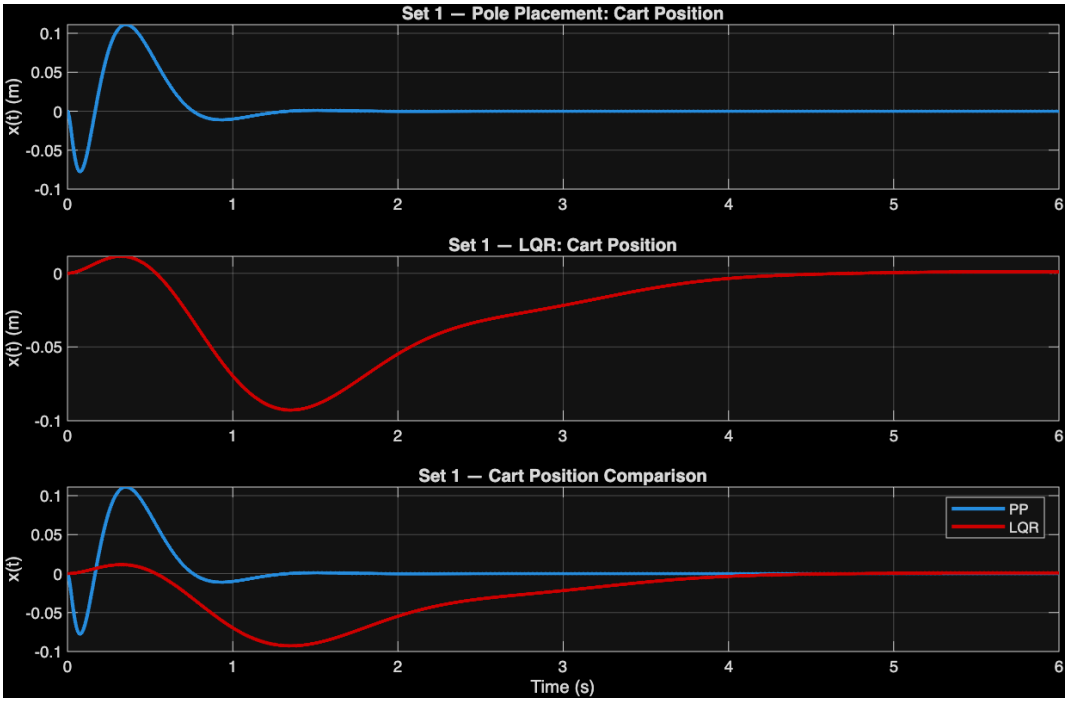

Figure 15: Set 1 (Long Pendulum): Cart position comparison between Pole Placement and LQR.

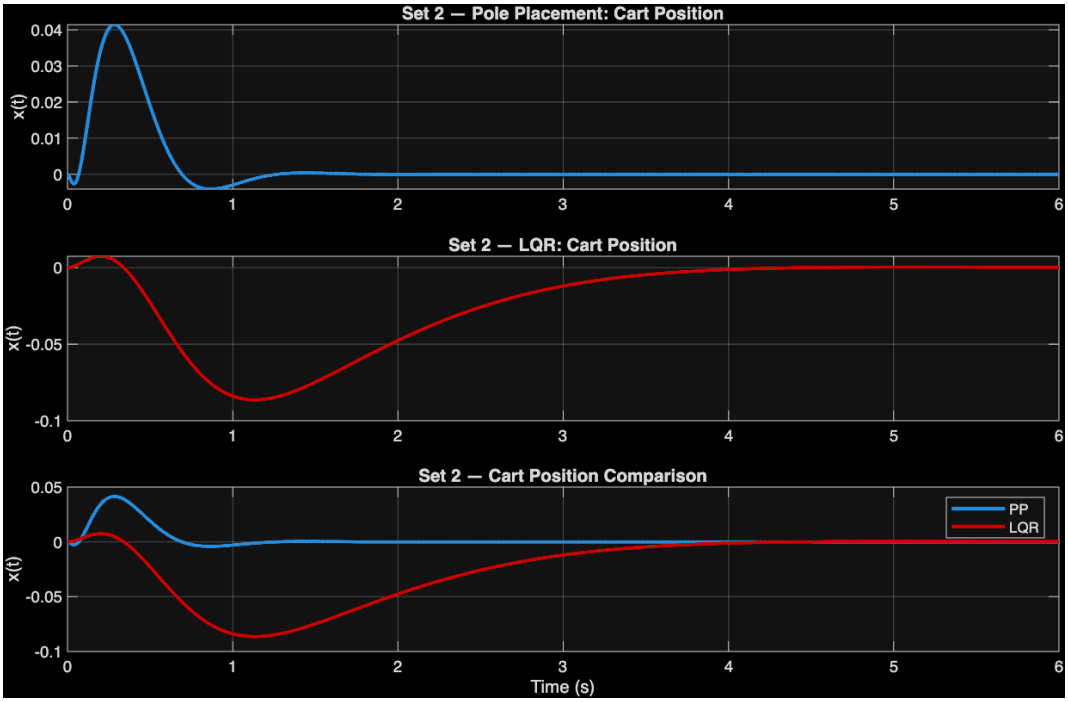

Figure 16: Set 2 (Short Pendulum): Cart position comparison between Pole Placement and LQR.

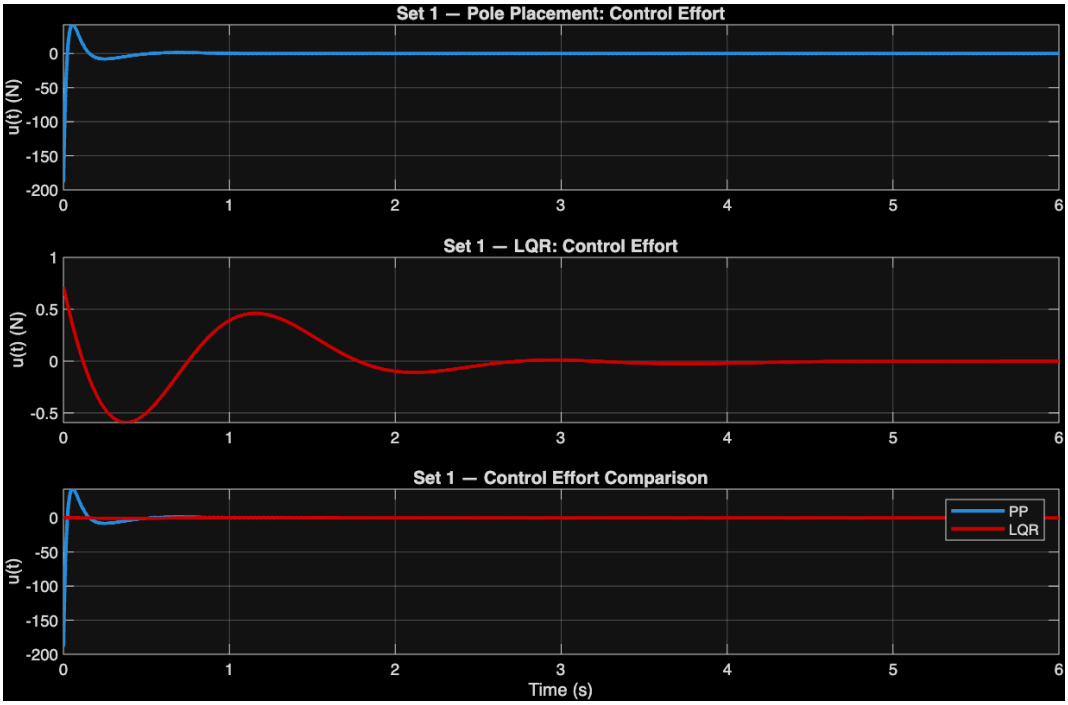

Figure 17: Set 1 (Long Pendulum): Control effort comparison between Pole Placement and LQR.

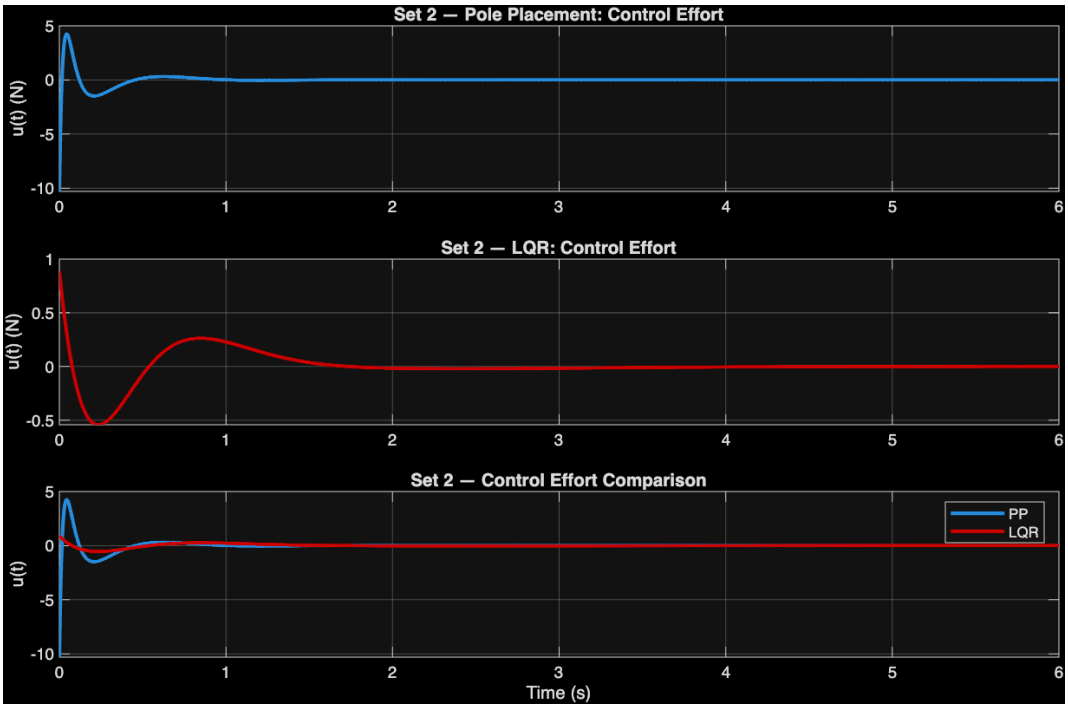

Figure 18: Set 2 (Short Pendulum): Control effort comparison between Pole Placement and LQR.

0.4 Discussion

The comparative results reveal consistent and physically meaningful trends across both parameter sets:

- **Pole Placement** achieves the fastest stabilization but requires extremely large and discontinuous control forces. Its performance is attractive in simulation but impractical for real IP02 hardware due to actuator saturation and mechanical limits.
- **LQR** produces significantly smoother, more energy-efficient, and more robust trajectories. It eliminates steady-state error with far smaller control effort, making it highly suitable for physical implementation.
- **The short pendulum (Set 2)** responds faster and requires less effort overall due to its stronger restoring torque, but the qualitative difference between controllers remains identical in both sets.

Overall, the simulations demonstrate that while Pole Placement can achieve extremely fast convergence, LQR provides the most balanced and realistic control action when physical constraints are considered.

Conclusion

This project developed a complete workflow for modeling, linearizing, and controlling the Quanser IP02 inverted pendulum system. Beginning from the nonlinear equations of motion, reduced and full-state linear models were constructed to support a range of controller designs. The investigation demonstrated how controller structure, model complexity, and physical constraints combine to shape closed-loop performance.

The study also emphasized the importance of aligning controller design with system limitations. The reduced two-state model allowed the PID controller to perform well in simulation but revealed why such simplified designs cannot stabilize the full pendulum– cart system. In contrast, full-state feedback methods—Pole Placement and LQR—provided feasible stabilization, with their performance directly tied to their underlying design philosophies.

Pole Placement delivered rapid stabilization but required unreasonably large and impulsive control inputs, demonstrating the gap between mathematical feasibility and hardware practicality. LQR, on the other hand, balanced state regulation and energy minimization, producing smooth, robust, and hardware-compatible trajectories across both parameter sets.

Taken together, these results provide a clear understanding of inverted pendulum control in both theory and practice. The modeling and control framework established here forms a strong foundation for future work, including nonlinear controllers, observer design, optimal trajectory planning, robust and adaptive methods, and eventual implementation on the physical Quanser IP02 platform.